Article

Theoretical Models on the Cu2O2 Torture Track: Mechanistic Implications for Oxytyrosinase and Small-Molecule Analogues

CRAMER, Christopher J., *et al*.

Abstract

Accurately describing the relative energetics of alternative bis(μ-oxo) and μ-η2:η2 peroxo isomers of Cu2O2 cores supported by 0, 2, 4, and 6 ammonia ligands is remarkably challenging for a wide variety of theoretical models, primarily owing to the difficulty of maintaining a balanced description of rapidly changing dynamical and nondynamical electron correlation effects and a varying degree of biradical character along the isomerization coordinate. The completely renormalized coupled-cluster level of theory including triple excitations and extremely efficient pure density functional levels of theory quantitatively agree with one another and also agree qualitatively with experimental results for Cu2O2 cores supported by analogous but larger ligands. Standard coupled-cluster methods, such as CCSD(T), are in most cases considerably less accurate and exhibit poor convergence in predicted relative energies. Hybrid density functionals significantly underestimate the stability of the bis(μ-oxo) form, with the magnitude of the error being directly proportional to the percentage Hartree−Fock exchange in the functional. [...]

Reference

CRAMER, Christopher J., *et al*. Theoretical Models on the Cu2O2 Torture Track: Mechanistic Implications for Oxytyrosinase and Small-Molecule Analogues. *The journal of physical chemistry. A*, 2006, vol. 11, no. 5, p. 1991-2004

DOI : 10.1021/jp056791e

Theoretical Models on the Cu_2O_2 Torture Track: Mechanistic Implications for Oxytyrosinase and Small-Molecule Analogues

Christopher J. Cramer,*,† Marta Włoch,‡ Piotr Piecuch,‡,§ Cristina Puzzarini,|| and Laura Gagliardi⊥

Department of Chemistry and Supercomputer Institute, University of Minnesota, 207 Pleasant St. SE, Minneapolis, Minnesota 55455, Department of Chemistry, Michigan State University, East Lansing, Michigan 48824, Department of Physics and Astronomy, Michigan State University, East Lansing, Michigan 48824, Dipartimento di Chimica "G. Ciamician", Universitá di Bologna, Via F. Selmi 2, I-40126 Bologna, Italy, and Department of Physical Chemistry, Sciences II University of Geneva, 30 Quai Ernest Ansermet, CH-1211 Geneva 4, Switzerland

Received: November 23, 2005

Accurately describing the relative energetics of alternative bis(μ-oxo) and μ-η^2:η^2 peroxo isomers of Cu_2O_2 cores supported by 0, 2, 4, and 6 ammonia ligands is remarkably challenging for a wide variety of theoretical models, primarily owing to the difficulty of maintaining a balanced description of rapidly changing dynamical and nondynamical electron correlation effects and a varying degree of biradical character along the isomerization coordinate. The completely renormalized coupled-cluster level of theory including triple excitations and extremely efficient pure density functional levels of theory quantitatively agree with one another and also agree qualitatively with experimental results for Cu_2O_2 cores supported by analogous but larger ligands. Standard coupled-cluster methods, such as CCSD(T), are in most cases considerably less accurate and exhibit poor convergence in predicted relative energies. Hybrid density functionals significantly *underestimate* the stability of the bis(μ-oxo) form, with the magnitude of the error being directly proportional to the percentage Hartree−Fock exchange in the functional. Single-root CASPT2 multireference second-order perturbation theory, by contrast, significantly *overestimates* the stability of bis(μ-oxo) isomers. Implications of these results for modeling the mechanism of C−H bond activation by supported Cu_2O_2 cores, like that found in the active site of oxytyrosinase, are discussed.

Introduction

Various metalloenzymes containing one, two, or more copper atoms activate molecular oxygen to oxidize organic substrates.[1−8] Tyrosinase is one such enzyme: a so-called type 3 copper protein, it oxidizes tyrosine residues to their corresponding *o*-quinones within an active site containing two copper atoms, both of which are involved in the oxidation reaction.[1,5,6,9] At least in part to better understand the mechanism of tyrosinase, an enormous amount of effort has gone into the study of the structures, spectroscopy, and reactivities of 2:1 Cu/O_2 model systems.[2,10−14]

The variety of ways in which two supported copper(I) atoms can bind O_2 turns out to be surprisingly rich (Figure 1).[12,15] The three dominant structural motifs that have been characterized experimentally are the trans end-on μ-η^1:η^1 peroxo, the side-on μ-η^2:η^2 peroxo, and the bis(μ-oxo), although select examples of the other three cases shown in Figure 1 have been identified or inferred. In the first two cases, the O_2 fragment is reduced to a peroxide dianion by oxidation of the two copper atoms to Cu(II). In the third case, the O−O bond is broken and the formal oxidation states of the core atoms are Cu(III) and O^{2-}. In general, the particular Cu_2O_2 motif observed is strongly dependent on the nature of the ligands. Thus, for example, tetradentate ligands tend to favor end-on peroxo binding, bidentate ligands favor bis(μ-oxo) as they ideally accommodate the preferred square-planar ligand arrangement for Cu(III), and binding motifs associated with tridentate ligands tend to vary depending on the rigidity and/or steric requirements of the ligand itself.[12,15] Indeed, for selected sets of ligands, it has been demonstrated that more than one motif can be accessed. For example, Jung et al.[16] have demonstrated that the binding of oxygen to a dicopper complex supported by a bridging *N,N,N′,N′*-bis{2-(2-pyridyl)ethyl}-1,4-butanediamine ligand shows a kinetic preference for end-on peroxo but a thermodynamic preference for side-on peroxo.

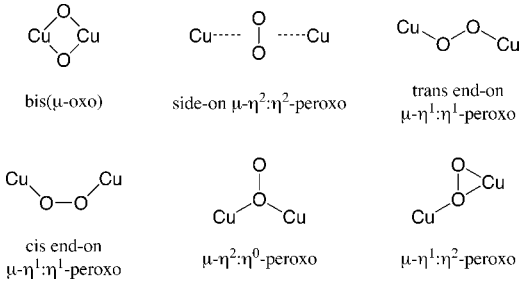

Figure 1. Binding motifs for Cu_2O_2.

Another example that has received special attention involves ligands that permit access to both the side-on peroxo and bis-

* To whom correspondence should be addressed. E-mail: cramer@pollux.chem.umn.edu.
† University of Minnesota.
‡ Department of Chemistry, Michigan State University.
§ Department of Physics and Astronomy, Michigan State University.
|| Universitá di Bologna.
⊥ Sciences II University of Geneva.

10.1021/jp056791e CCC: $33.50
Published on Web 01/06/2006

(μ-oxo) forms.[11,13,17] The former geometry has been shown by X-ray crystallography to be present in oxyhemocyanin, an oxygen-transporting protein with the imidazole rings of six histidine residues serving as ligands.[18,19] Although no X-ray crystal structure has yet been obtained for oxytyrosinase, spectral data for oxyhemocyanin and oxytyrosinase are sufficiently similar that there is little doubt that the resting state of oxytyrosinase also involves a side-on μ-η^2:η^2 peroxo with five or six histidine ligands.[6] However, Tolman and co-workers,[11,13,17,20,21] and later others,[22−26] have demonstrated that in select instances the relative energies of isomeric μ-η^2:η^2 peroxo and bis(μ-oxo) complexes can be sufficiently close to one another, and the barrier to their interconversion sufficiently low, that the two species may be in rapid equilibrium with one another; theoretical studies have rationalized many of the electronic structural details governing this phenomenon.[27−34] This observation potentially complicates mechanistic analysis in model systems and, by extension, oxytyrosinase, because the kinetics for systems characterized by a rapid preequilibrium can be indistinguishable from systems involving only a single reactant.[35] Thus, even in the absence of observing a spectral signature for a bis(μ-oxo) intermediate, because it is present at, say, part per million concentration, one cannot a priori discount the possibility that this same isomer is so much more reactive than the μ-η^2:η^2 peroxo that product derives predominantly from prior isomerization and subsequent reaction.

Notwithstanding this complication, a sufficient number of model compounds presenting the various motifs have now been examined such that general reactivity trends have been associated with each one.[12,13,17,36] In particular, end-on peroxo species have been characterized as basic (subject to protonation to generate hydrogen peroxide) and nucleophilic (reactive with acylating agents) but not particularly electrophilic (no oxidation of phosphines to phosphine oxides). Side-on peroxo compounds, by contrast, fail to exhibit basic character and enhance the electrophilicity of the bound O_2 fragment, as judged by their abilities to abstract H atoms from good donors, oxidize phosphines to phosphine oxides, and hydroxylate aromatic rings both intra- and intermolecularly. Finally, bis(μ-oxo) compounds have been demonstrated also to be nonbasic and to be strongly electrophilic, oxidizing both activated and aliphatic C−H bonds, hydroxylating aromatic rings, and serving as oxidizing agents in electron-transfer reactions.

Given the complications alluded to above with respect to distinguishing between direct reactivity and prior equilibration (and, of course, the possibility that *both* these pathways may be kinetically competitive), computational protocols have also been brought to bear to characterize energetic and mechanistic details for particular reactions. Studies of C−H bond activation by bis(μ-oxo) compounds have documented that this motif engages directly in H-atom transfer/rebound type mechanisms.[37−39] A very recent density functional study also found a transition-state structure for hydroxylation of a coordinated phenolate by a bis(μ-oxo) species.[40] With respect to oxytyrosinase itself, Siegbahn has examined in considerable detail possible reactions of a side-on peroxo species coordinated by six imidazole ligands with either phenol or phenolate.[41−43] Siegbahn found that the coordination of phenolate to copper causes the side-on μ-η^2:η^2 peroxo species to distort to a μ-η^2:η^1 geometry, which may either react directly itself or may further decoordinate to a μ-η^2:η^0 peroxyl radical species that acts as the electrophilic species (the relative energies of the two species were within the estimated error range of the calculations, hence the qualification as to which, if either, is more mechanistically relevant).[43]

CHART 1

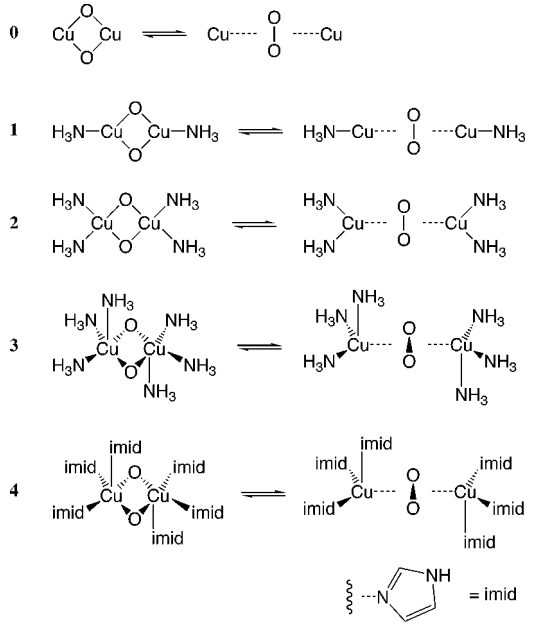

Implicit in several of the theoretical studies described above is the assumption that the energy difference between the bis(μ-oxo) and μ-η^2:η^2 peroxo motifs is accurately predicted by the particular level of theory employed. However, no prior calculation has tested its employed theory in a *quantitative* fashion against an experimentally characterized bis(μ-oxo)/μ-η^2:η^2 peroxo equilibrium, nor has it been possible to demonstrate convergence of a suitably complete level of electronic structure theory for a model system more simply ligated than an experimentally characterized system to establish a benchmark against which to compare other more practical levels of theory.

In this work, we compare several different density functional (DFT) models, the single-root multireference second-order perturbation theory (CASPT2), and standard and completely renormalized (CR) coupled-cluster (CC) methods with respect to their abilities to predict accurate energetics for the conversion of the bis(μ-oxo) $Cu_2O_2^{2+}$ core to the μ-η^2:η^2 peroxo motif. We consider various ligand sets (Chart 1), including no ligands at all (**0**), one (**1**), two (**2**), and three (**3**) ammonia ligands per copper atom, and finally three imidazole ligands (**4**) per copper atom; the last ligand set is directly relevant to the case of oxytyrosinase. We find inter alia that (i) the CR-CC theory makes predictions that are reasonably well converged with respect to high-order correlation effects at the triple-excitation level and considerably more accurate than the results of standard CC calculations; (ii) single-root CASPT2 results are very sensitive to active-space choice and, even with large active spaces that provide relative isomer energies that are apparently converged with respect to the orbitals included, this level overestimates the stability of bis(μ-oxo) isomers relative to μ-η^2:η^2 peroxo isomers by 20−30 kcal mol^{-1}; and (iii) DFT models show extreme sensitivity to the incorporation of Hartree−Fock (HF) exchange: pure functionals provide quantitatively useful predictions but hybrid HF-DFT functionals, like the popular B3LYP model, underestimate the stability of bis(μ-oxo) isomers relative to μ-η^2:η^2 peroxo isomers by 5−10 kcal mol^{-1} for every 10% of HF exchange included in the functional. The consistency between CR-CC predictions and those from pure DFT func-

tionals for **0**−**3**, together with their mutual good agreement in the case of **3** with recently published[34] multireference configuration interaction (MRCI) data, strongly suggests that pure DFT functionals will provide accurate predictions for Cu_2O_2 systems with larger and more realistic ligands, like the oxytyrosinase-related case **4**, for which calculations at such levels as CR-CC or MRCI are not presently practical.

Theoretical Methods

Basis Sets. Four different basis sets were used in this work, which we designate BS1, BS2, BS3, and BS4. In all four sets, the Stuttgart pseudopotential and associated basis functions were used for Cu.[44] In BS1, the largest basis set, which was employed for most energy calculations, the atomic natural orbital (ANO) basis set of Pierloot et al.[45] was used. For N and O we used a [10s6p3d | 4s3p2d] contraction, whereas for H we used a [8s4p | 2s1p] contraction. In BS2, the same primitive functions were contracted as 3s2p1d and 1s, respectively. BS3 was used only for geometry optimizations of **3** and employed the Pople basis set 6-31G(d) for H, N, and O.[46] BS4 was used only for **4** and consisted of the Pople basis sets[46] STO-3G and 6-311G(d) for H and O, respectively, and the MIDI! basis set[47] for C and N.

Density Functionals. We assayed three different pure functionals. The BLYP functional combines the generalized-gradient approximation (GGA) exchange functional of Becke[48] with the GGA correlation functional of Lee, Yang, and Parr.[49] The *m*PWPW91 functional combines the GGA exchange[50] and correlation[51] functionals of Perdew and Wang as modified by Adamo and Barone.[52] The TPSS functional is a meta GGA functional.[53]

We also considered hybrid HF-DFT functionals.[54] The B3LYP,[55] *m*PW1PW91,[52] MPW1K,[56] and TPSSh[57] functionals incorporate 20%, 25%, 48.2%, and 10% HF exchange, respectively, into their corresponding functionals.

For singlet-state calculations, unstable restricted (R) self-consistent-field (SCF) solutions were reoptimized at the unrestricted (U) SCF level.[58] All restricted solutions were checked for instability. Singlet energies from unrestricted calculations were computed in two ways. First, the raw broken-spin-symmetry (BS) SCF energy was used without modification. Second, the sum method[59] was employed to eliminate spin contamination from the triplet state in the SCF solution. In this approach, the singlet energy is computed as[60−62]

$$E_{\text{singlet}} = \frac{2E_{\langle S_z\rangle=0} - \langle S^2\rangle E_{\langle S_z\rangle=1}}{2 - \langle S^2\rangle} \qquad (1)$$

where the triplet energy is computed for the single-determinantal high-spin configuration $S_z = 1$ (at the BS geometry) and $\langle S^2\rangle$ is the expectation value of the total-spin operator applied to the Kohn−Sham (KS) determinant for the unrestricted $S_z = 0$ calculation. Gräfenstein and Cremer[63] have shown that values of $\langle S^2\rangle$ computed at the DFT level have diagnostic value in assessing spin contamination; thus, the sumBS approach is more physically realistic than using the raw BS energy.

Single-Reference Post-SCF Levels. We performed a variety of standard single-reference CC calculations[64,65] using the CC method with singles and doubles (CCSD),[66−68] the CC method with singles, doubles, and noniterative triples (CCSD(T)),[69] and, to explore the role of higher-order correlations, the CC method with singles, doubles, and noniterative triples and quadruples (CCSD(TQ)), using variant "b" of the factorized CCSD(TQ) approximation.[70] However, although the CCSD, CCSD(T), and CCSD(TQ) methods offer a highly accurate treatment of dynamic correlation effects (particularly the last two), they usually fail, sometimes dramatically, in cases that require a well-balanced description of dynamical and nondynamical correlation effects, e.g., in systems that have a significant biradical character[71−73] and reaction paths involving significant bond stretching or breaking[74−84] (indeed, achieving such balance is challenging for *any* ab initio method—as shown below, even multireference techniques can have difficulties when a multidimensional reference space that is larger than present practical limits permit is required to treat different types of correlation on an equal footing).

To improve on the CC model, we performed calculations using the recently developed[70,74,75,82−84] completely renormalized CCSD(T) (CR-CCSD(T)) and CCSD(TQ) (CR-CCSD(TQ)) methods, which can accurately and effectively deal with reactive potential-energy surfaces involving bond stretching,[74−84] biradicals,[71−73] and other cases of electronic near-degeneracies within a single-reference description employing an RHF reference. We used variant "b" of the CR-CCSD(TQ) approach,[70] which enables us to determine if the CR-CCSD(T) results are reasonably well converged with respect to higher-order correlation effects. Although the CR-CCSD(T) and CR-CCSD(TQ) approaches provide a robust description of biradical systems, they slightly violate the rigorous size extensivity of the CC theory (at the level of 0.5−1.0% of the changes in the correlation energy along a reaction pathway). Also, certain types of high-order dynamic correlations, which are represented, for example, as disconnected products of singly, doubly, and triply excited clusters and which may or may not play a role in the systems examined in this study, are neglected at the CR-CCSD(T) level (as they are also in CCSD(T)). To address the issues of convergence with respect to higher-order correlations neglected in CR-CCSD(T) and size-extensivity, we also performed calculations using the recently proposed CR-CCSD(T)$_L$ approach, which is based on a new, biorthogonal formulation of the method of moments of CC equations (a formalism used to design all CR-CC methods[74,75,82,84]) employing the left eigenstates of the similarity-transformed Hamiltonian of CC theory.[85−87] The CR-CCSD(T)$_L$ method, also referred to as the CR-CC(2,3) approach,[86,87] is a rigorously size-extensive, improved variant of the CR-CCSD(T) approach, which describes the aforementioned higher-order correlations neglected in the CR-CCSD(T) calculations while eliminating the failures of standard CC methods, such as CCSD(T), in calculations involving single-bond breaking and biradicals. Additional details are available in the Supporting Information.

In all single-reference correlated calculations, we used the RHF determinant as a reference. The RHF, second-order many-body perturbation theory (MBPT(2) or MP2), CCSD(T), CR-CCSD(T), and CR-CCSD(T)$_L$ calculations were performed for all systems up to **3**. The smaller BS2 basis set was used for CR-CCSD(T)$_L$ calculations on **3** (all other CC and CR-CC calculations were carried out with BS1). Because of resource demands, CR-CCSD(TQ)/BS1 calculations were carried out for **0** and **1** only. We explicitly correlated the 4s and 3d electrons of the Cu atoms, the 2s and 2p electrons of the N and O atoms, and the 1s electrons of the H atoms. For the bare system **0**, we also computed CR-CCSD(T)$_L$ results after adding the 12 3p electrons of the Cu atoms to those being correlated.

Multireference SCF and Post-SCF Levels. The complete active-space (CAS) SCF method[88] was used to generate molecular orbitals (MOs) and reference functions for subsequent multiconfigurational second-order perturbation calculations of the dynamic correlation energy (CASPT2).[89] Unless stated

otherwise, it is implicit in this paper that CASSCF refers to the optimization of the *ground-state* MOs (i.e., there is no state averaging including excited states) and CASPT2 refers also to the application of the model only to the *ground state* without permitting any sort of multistate mixing involving higher-energy roots. Full details of orbital selections, energies, and configuration and reference weights are provided in the Supporting Information—we report here only the most critical details.

The performance of the CASSCF/CASPT2 model, which has been widely used for the quantitative modeling of various aspects of transition-metal chemistry,[90−92] depends critically on the choice of orbital active space for the CAS reference. To better describe our active spaces, we will adhere to a convention whereby the z axis of a Cartesian frame is defined by the Cu−Cu vector, the y axis is defined by the O−O vector, and the x axis is then orthogonal to the Cu_2O_2 core. Although full details for *all* spaces are available in the Supporting Information, it is appropriate here to be explicit about our largest active space for **3** because of the prior work on this system at the CASPT2 level by Flock and Pierloot.[30] These authors first considered an (8,10) active space comprised of the σ and σ^* orbitals dominated by appropriate combinations of the O $2p_y$ basis functions, the bonding and antibonding combinations of the $3d_{yz}$ basis functions from each Cu, two sets of formally π and π^* orbitals dominated by appropriate combinations of O $2p_z$ (occupied) and $3p_z$ (correlating virtual) basis functions, an additional σ_{OO} virtual orbital dominated by O $3p_y$ basis functions, and an unspecified linear combination of Cu $4d_{yz}$ basis functions. Flock and Pierloot[30] further expanded this to a (12,14) active space by adding two sets of formally π and π^* orbitals dominated by appropriate combinations of O $2p_x$ (occupied) and $3p_x$ (correlating virtual) basis functions. In our case for **3**, we found after extensive analysis that two of the virtual orbitals in this (12,14) space were not particularly helpful, namely the $4d_{yz}$ combination and the π^* orbital formed from $3p_z$ basis functions. In their place, we included 2 occupied orbitals (generating a (16,14) active space) dominated by bonding and antibonding combinations of O 2s orbitals. A graphical depiction of the (16,14) active space for **3** is also available as Supporting Information. We also considered a still larger (14,15) active space (generating 5179830 Slater determinants for the singlet ground state) which led to similar results, suggesting that, in this case (and analogously for **0**−**2**), the CASSCF and CASPT2 results are well converged with respect to further expansion of the active space, at least within practical limits, which do not permit further expansion to a full-valence active space.

Two sets of CASPT2 calculations followed each CASSCF calculation. In the first, the O 1s and Cu 2s and 3s orbitals were kept frozen. In the second, the Cu 3p orbitals were also kept frozen. All CASPT2 calculations employed a real level shift[93] of 0.1 au in combination with a new technique[94] that shifts active orbital energies to simulate ionization energies for orbitals excited out of and electron affinities for orbitals excited into the active space. In the cases examined here, however, intruder states did not appear to pose any significant problems.

Geometries. For systems **0**, **1**, and **2**, idealized bis(μ-oxo) and μ-η^2:η^2 peroxo core geometries were generated. For the former motif, the Cu−Cu and O−O distances in the D_{2h} core were taken as 2.8 and 2.3 Å, respectively. For the latter motif, these same distances were taken to be 3.6 and 1.4 Å, respectively. For **1**, ammonia ligands were added to each Cu along the Cu−Cu axis with Cu−N distances of 2.0 Å, N−H distances of 1.0 Å, CuNH angles of 110°, and OCuNH dihedral angles consistent with the C_{2h} point group. For **2**, all internal coordinates were the same as for **1** except that the N atoms were placed so as to make NCuCu angles of 135° and each ammonia ligand had one N−H bond eclipsing a Cu−O bond, thereby generating a structure belonging to the D_{2h} point group. For **3**, the geometries of both motifs were optimized at the B3LYP/BS3 level (R and U for the bis(μ-oxo) and μ-η^2:η^2 peroxo cases, respectively) within the C_{2h} point group. For **4**, geometries were fully optimized within the C_{2h} and C_i point groups at both the R and U BLYP/BS3 and B3LYP/BS3 levels.

Intermediate geometries along linear isomerization paths were generated for **0**−**3** according to

$$q_i(F) = q_i(0) + \frac{F}{100}[q_i(100) - q_i(0)] \qquad (2)$$

where q_i is a given atomic Cartesian coordinate and F is the fraction of progress along the isomerization coordinate (so that 0 and 100 define the bis(μ-oxo) and μ-η^2:η^2 peroxo geometries, respectively). We present results for F values of 0, 20, 40, 60, 80, and 100. Reference to a particular structure along an isomerization coordinate will henceforth be made by adding F as a subscript to the structure cardinal; e.g., $\mathbf{2}_{20}$ refers to the structure 20% converted from $\mathbf{2}_0$ to $\mathbf{2}_{100}$.

In the case of **4**, additional end-on μ-η^1:η^1 peroxo geometries in the C_i point group were obtained from full optimization at the R and U BLYP/BS4 and B3LYP/BS4 levels. The natures of all stationary points for **4** were confirmed by the calculation of analytic force constants.

Software. Full details on software are provided in the Supporting Information.

Results

$Cu_2O_2^{2+}$. The energies for structures of **0** as a function of F were computed at all levels of theory using the BS1 basis set. At the CAS and CASPT2 levels, an (8,8) and a large (16,14) active space were employed. At the DFT level, restricted solutions to the Kohn−Sham SCF equations could not be successfully converged for the pure functionals BLYP, *m*PWPW91, and TPSS, although they could be for the hybrid functionals. However, even those RDFT solutions that *could* be converged were all unstable to symmetry breaking (computed $\langle S^2 \rangle$ values for the KS determinants ranged from 0.4 to 1.0 depending on structure and functional). Electronic energies at many levels relative to $\mathbf{0}_{100}$ are provided in Table 1. Absolute electronic energies and a more complete list of relative energies, BS-DFT $\langle S^2 \rangle$ values, and $^3B_{2g}$ electronic energies for all structures (the final two quantities are required to compute sumBS-DFT energies) may be found in the Supporting Information.

A considerable variation in relative energies as a function of theoretical level is observed. For $\mathbf{0}_0$, the predicted relative energy ranges over more than 90 kcal mol^{-1}! Figure 2 presents predicted structural relative energies graphically for select levels of theory. Table 1 and Figure 2 indicate that the CR-CC results are reasonably well converged, both with respect to the effect of higher-than-triple excitations (quadruples play a small role) and additional correlations involving triply excited clusters, brought by the size-extensive CR-CCSD(T)$_L$ approach. There is a very good agreement between the CR-CC and pure DFT results. CASSCF and CASPT2 produce energies which are considerably below those obtained with the CR-CC and pure DFT approaches, and there is little substantive difference between the (8,8) and (16,14) active-space results. Unlike CR-CC, the standard CC approaches do not produce the well-converged results and seem to fail in the biradical $F = 60-$

TABLE 1: Relative Energies (kcal mol^{-1}) of $\mathbf{0}_F$ Structures with BS1[a]

	F							*F*					
level of theory	0%	20%	40%	60%	80%	100%	level of theory	0%	20%	40%	60%	80%	100%
RHF	98.0	91.4	80.7	60.5	32.0	0.0	B3LYP	52.3	44.1	35.6	24.0	10.1	0.0
MP2	29.0	9.0	−5.5	−12.9	−11.8	0.0	BS-B3LYP	52.9	47.6	40.6	29.3	14.0	0.0
CCSD	41.1	33.9	26.3	16.9	7.2	0.0	sumBS-B3LYP	56.7	47.6	37.6	25.1	10.6	0.0
CCSD(T)	30.6	22.2	13.5	5.3	0.0	0.0	*m*PWPW91[c]						
CR-CCSD(T)	36.9	28.6	20.7	11.9	3.7	0.0	BS-*m*PWPW91	39.7	36.1	30.8	21.8	9.7	0.0
CR-CCSD(T)$_L$	35.5	26.1	17.6	9.4	2.4	0.0	sumBS-*m*PWPW91	42.3	36.4	29.3	19.4	7.6	0.0
	(40.3)	(30.7)	(21.8)	(12.6)	(4.2)	(0.0)	*m*PW1PW91	59.0	50.2	40.9	28.1	12.5	0.0
CCSD(TQ)	21.7	14.4	7.6	1.6	−1.9	0.0	BS-*m*PW1PW91	60.0	54.3	46.5	33.9	16.8	0.0
CR-CCSD(TQ)	35.1	26.7	18.9	10.7	3.1	0.0	sumBS-*m*PW1PW91	66.3	55.6	43.8	29.3	13.0	0.0
CR-CCSD(TQ)$_L$[b]	38.5	28.8	20.0	11.4	3.6	0.0	MPW1K	70.9	61.7	51.3	36.3	17.3	0.0
CAS(8,8)	−3.6	−11.1	−16.5	−19.5	−16.7	0.0	BS-MPW1K	74.0	67.4	58.2	43.1	22.4	0.0
CAS(16,14)	0.2	−7.2	−12.7	−16.3	−14.0	0.0	sumBS-MPW1K	89.3	72.4	55.8	37.2	17.4	0.0
CASPT2(8,8)	6.5	0.4	−3.1	−5.8	−6.1	0.0	TPSS[c]						
	(6.0)	(0.5)	(−2.3)	(−4.6)	(−4.8)	(0.0)	BS-TPSS	39.6	35.5	29.8	20.5	8.7	0.0
CASPT2(16,14)	1.4	−2.7	−5.4	−7.6	−8.7	0.0	sumBS-TPSS	42.4	35.8	28.3	18.3	6.8	0.0
	(7.2)	(1.9)	(−0.6)	(−2.7)	(−3.4)	(0.0)	TPSSh	48.5	39.8	31.2	20.2	7.7	0.0
BLYP[c]							BS-TPSSh	47.8	42.7	36.0	25.3	11.6	0.0
BS-BLYP	36.0	32.6	27.8	19.4	8.2	0.0	sumBS-TPSSh	50.9	42.9	33.9	22.2	8.9	0.0
sumBS-BLYP	38.5	32.8	26.1	17.0	6.2	0.0							

[a] Values in parentheses correlate all valence electrons and the Cu 3p electrons (44 total), whereas all other single-reference and CASPT2 correlated values refer to the correlation of only the valence electrons (32 total). [b] Computed as CR-CCSD(T)$_L$ + {CR-CCSD(TQ) − CR-CCSD(T)} where the CR-CCSD(T)$_L$ value for 44 correlated electrons was used. [c] Restricted solutions could not be converged.

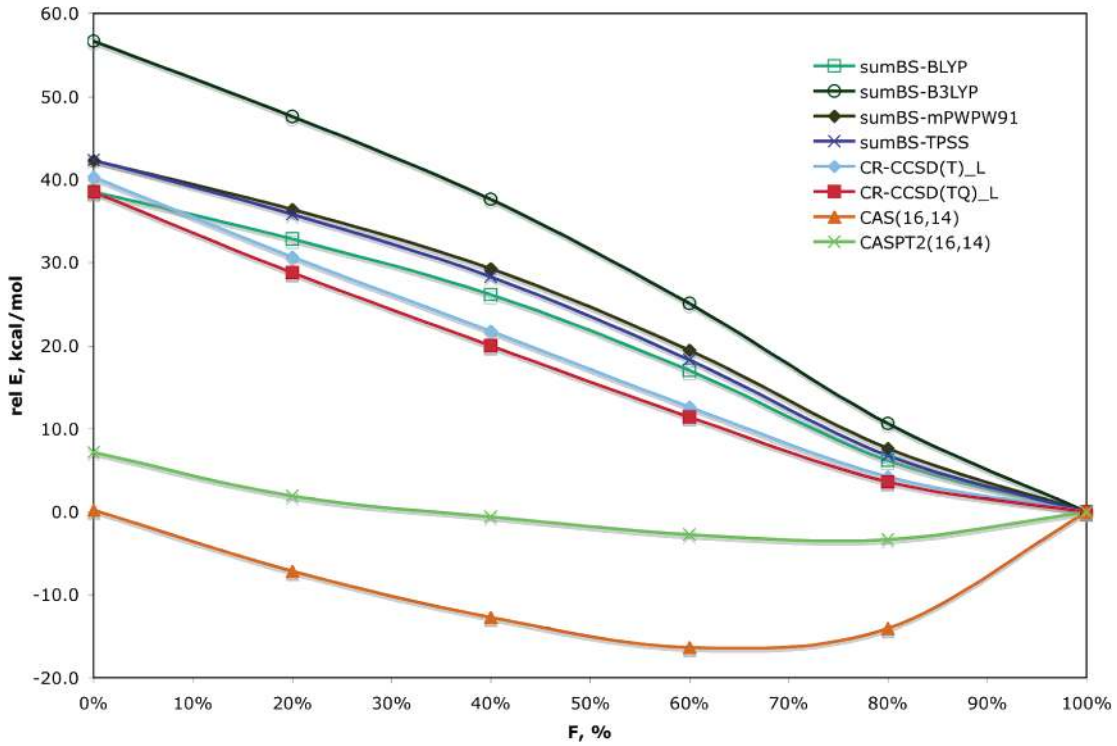

Figure 2. Relative energy (kcal mol^{-1}) vs *F* for **0** at select levels of theory. (Inset) Legend.

100 region. In particular, the CCSD(TQ) method stabilizes the $F = 80$ structure. This is a sign of the failure of the standard noniterative CC methods, which often artificially lower the energies in biradical regions.

Figure 3 illustrates the nominal $2b_{1g}$ HOMO and $3b_{3g}$ LUMO orbitals from RB3LYP calculations (which become mixed at the BS-DFT level) for the $\mathbf{0}_0$ and $\mathbf{0}_{100}$ structures; the relative energies of the HOMO and LUMO orbitals for $\mathbf{0}_0$ were found to be sensitive to the functional (they are reversed for TPSSh, for example), consistent with the strong preference for broken-symmetry DFT solutions. Figure 3 depicts some other key orbitals as well. The occupied/virtual pairs $2b_{3g}/3b_{3g}$ and $4b_{2u}/5b_{2u}$ are the MOs whose occupation numbers differ most significantly from 0 or 2 in the CAS calculations (the CAS orbitals are very similar in shape to the DFT orbitals), and their occupations are moreover observed to change significantly along the isomerization coordinate. In particular, the $2b_{3g}/3b_{3g}$ and $4b_{2u}/5b_{2u}$ occupation numbers are 1.79/0.55 and 1.50/0.39 in $\mathbf{0}_0$ and 1.98/0.69 and 1.32/0.06 in $\mathbf{0}_{100}$. Thus, as the system isomerizes from bis(μ-oxo) to μ-η^2:η^2 peroxo and a formal O−O bond is formed, there is a transfer of about 0.5 electrons out of those MOs that combine the Cu d_{xy} orbitals with the σ^*_{OO} orbital into those MOs that combine the same Cu orbitals with the O p_z orbitals. This same transfer is observed in the analogous orbitals for **1**−**3** (data in Supporting Information) and is

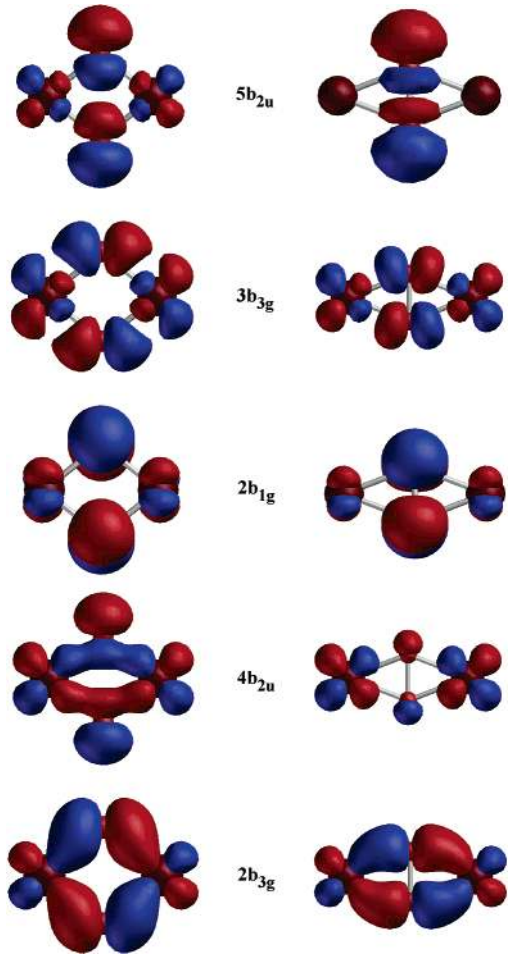

Figure 3. B3LYP/BS1 orbitals for $\mathbf{0}_0$ (left) and $\mathbf{0}_{100}$ (right), respectively.

illustrative of the sensitivity of the CAS wave functions to the Cu_2O_2 structure.

{(NH$_3$)Cu}$_2$O$_2^{2+}$. The energies for structures of **1** as a function of F were computed at all levels of theory using the BS1 basis set. At the CAS and CASPT2 levels, a (16,14) active space was employed. At the DFT level, restricted solutions to the Kohn−Sham SCF equations could be obtained for all functionals, but they were all unstable to symmetry breaking (computed $\langle S^2 \rangle$ values for the KS determinant ranged from 0.2 to 1.0 depending on structure and functional). In the interests of brevity, we list in Table 2 relative energies at only the most representative levels of theory and report in the Supporting Information all absolute and relative electronic energies, BS-DFT $\langle S^2 \rangle$ values, and ^3A_g electronic energies for all structures.

Similar to **0**, the variation in relative energies as a function of theoretical level is very large: just under 80 kcal mol^{-1} for $\mathbf{1}_0$. As is the case for **0**, the predicted relative energy for the bis(μ-oxo) structure ($F = 0$) is lowest at the CASPT2 level and very high at hybrid DFT levels incorporating large amounts of HF exchange. In addition, the CR-CC and pure DFT predictions are found to be intermediate between these high and low extremes and relatively close one to another. As shown in Table 2 and Figure 4, the CR-CC results are again well converged with respect to higher-order correlations, and no significant differences are observed between the CR-CCSD(T) and CR-CCSD(T)$_L$ results. This should be contrasted with the results of the CCSD(T) and CCSD(TQ) calculations, which are quite different from one another and display relatively deep minima in the $F = 80$ region, indicating the failure of the standard noniterative CC approximations in the biradical region.

TABLE 2: Relative Energies (kcal mol^{-1}) of $\mathbf{1}_F$ Structures with BS1[a]

	F					
level of theory	0%	20%	40%	60%	80%	100%
CCSD(T)	23.9	16.2	7.8	−0.8	−4.8	0.0
CR-CCSD(T)	28.4	20.2	12.9	5.1	−0.7	0.0
CR-CCSD(T)$_L$	30.6	21.1	12.5	3.8	−1.6	0.0
CCSD(TQ)	12.3	5.0	−1.2	−6.7	−7.8	0.0
CR-CCSD(TQ)	28.0	19.4	12.1	4.6	−0.9	0.0
CR-CCSD(TQ)$_L$[b]	30.2	20.4	11.7	3.3	−1.8	0.0
CAS(16,14)	13.8	5.4	−3.1	−11.1	−13.2	0.0
CASPT2(16,14)	−0.2	−6.9	−8.5	−11.8	−11.6	0.0
	(−1.5)	(−8.3)	(−8.8)	(−11.7)	(−11.4)	(0.0)
sumBS-BLYP	36.8	32.3	25.0	16.4	7.1	0.0
sumBS-B3LYP	50.8	39.1	24.7	8.5	−0.6	0.0
sumBS-*m*PWPW91	40.8	33.2	25.9	16.8	6.0	0.0
sumBS-TPSS	39.9	32.0	24.4	15.3	5.0	0.0

[a] Values in parentheses correlate all valence electrons and the Cu 3p electrons (44 total), whereas all other non-DFT values refer to correlation of only the valence electrons (32 total). [b] Computed as CR-CCSD(T)$_L$ + {CR-CCSD(TQ) − CR-CCSD(T)}.

The key MOs from RDFT and CAS calculations are essentially identical to those presented in Figure 3 for $\mathbf{0}_0$ and $\mathbf{0}_{100}$, with no significant contributions from basis functions associated with the ammonia ligands (by symmetry, the N p_z orbitals used in bonding to copper cannot mix with the orbitals in Figure 3). In terms of electronic structure and isomerization energetics, **0** and **1** are very similar.

{(NH$_3$)$_2$Cu}$_2$O$_2^{2+}$. The energies for structures of **2** as a function of F were also computed at all levels of theory using the BS1 basis set, except that consideration of quadruple excitations was no longer practical at the CC levels. At the CAS and CASPT2 levels, a (16,14) active space was used. At the DFT level, restricted solutions to the Kohn−Sham SCF equations could be obtained for all functionals. With the pure DFT functionals, the RDFT solutions were stable to spin-symmetry breaking. With the hybrid functionals, on the other hand, all structures with $F \geq 40$ were unstable to symmetry breaking, and with the *m*PW1PW91 and MPW1K functionals, the $F = 0$ and $F = 20$ solutions were also found to be unstable. Representative relative energies are provided in Table 3, and absolute electronic energies, BS-DFT $\langle S^2 \rangle$ values, and triplet electronic energies for all structures at all levels of theory are provided in the Supporting Information.

Although reduced somewhat from the magnitude seen for the cases of **0** and **1**, the variation in relative energies as a function of theoretical level remains large for **2**: nearly 60 kcal mol^{-1} for $\mathbf{2}_0$. As shown in Figure 5 and Table 3, the CR-CC and pure DFT levels still agree fairly well one with another, but these levels now predict the energy for $\mathbf{2}_0$ either to be somewhat below the relative zero assigned to $\mathbf{2}_{100}$ (CR-CCSD(T) and pure DFT) or to be essentially equal to it (CR-CCSD(T)$_L$). Increased HF character in hybrid functionals continues to be associated with rapidly increasing relative energies for $\mathbf{2}_0$ and other structures having low values of F. The CAS and CASPT2 predictions continue to be in poor agreement with the CR-CC and pure DFT results, with CASPT2 predicting anomalously low relative energies for $\mathbf{2}_0$.

The frontier molecular orbitals from RDFT calculations for **2** are substantially perturbed in relative energy compared to **0** and **1** by the ammonia ligands now found in the regions of maximum amplitude of the Cu d_{xy} orbitals. In the case of the μ-η^2:η^2 peroxo structure ($F = 100$) at the B3LYP level, the orbitals analogous to $4b_{2u}$ and $3b_{3g}$ in Figure 3 are predicted to be the HOMO−1 and LUMO, respectively. Both of these two

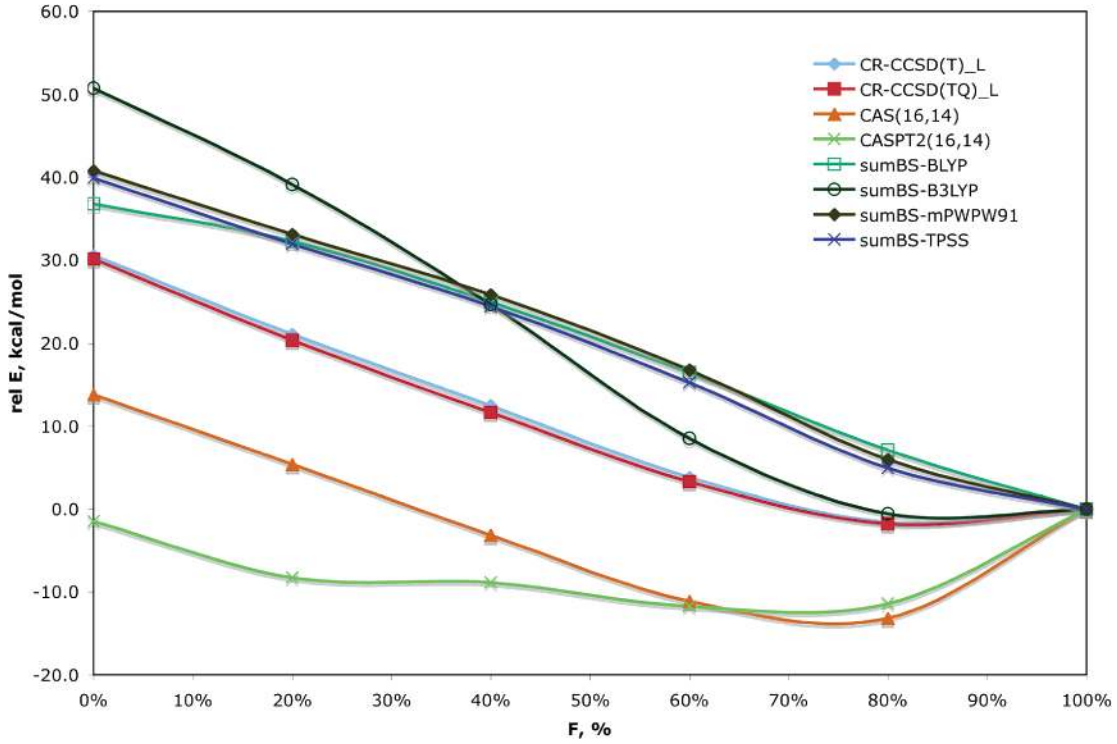

Figure 4. Relative energy (kcal mol^{-1}) vs F for **1** at select levels of theory. (Inset) Legend.

TABLE 3: Relative Energies (kcal mol^{-1}) of 2_F Structures with BS1[a]

	F					
level of theory	0%	20%	40%	60%	80%	100%
CCSD(T)	−5.2	−3.7	0.0	−3.3	−7.1	0.0
CR-CCSD(T)	−3.7	−2.5	1.0	−0.4	−4.3	0.0
CR-CCSD(T)$_L$	0.4	1.0	2.4	−0.9	−4.7	0.0
CAS(16,14)	3.7	0.0	−1.8	−7.0	−11.2	0.0
CASPT2(16,14)	−21.9	−20.9	−15.1	−10.7	−10.6	0.0
	(−25.1)	(−23.5)	(−16.7)	(−11.1)	(−10.6)	(0.0)
BLYP	−5.1	−3.1	0.7	2.0	−1.3	0.0
sumBS-B3LYP	14.9	17.5	20.4	7.1	−0.3	0.0
*m*PWPW91	−2.4	−0.4	3.0	3.7	−0.3	0.0
TPSS	−3.8	−1.8	1.5	2.1	−1.5	0.0

[a] Values in parentheses correlate all valence electrons and the Cu 3p electrons (44 total), whereas all other non-DFT values refer to the correlation of only the valence electrons (32 total).

MOs continue to include a large contribution from the Cu d_{xy} atomic orbitals (AOs) so that a broken-symmetry solution that mixes them permits magnetic exchange, such that a single-determinant method like KS DFT can effectively represent a biradical situation like that associated with two formal Cu(II) atoms, each one of which has one spin localized upon it. The corresponding orbitals may be found in the occupied and virtual manifolds, respectively, for the bis(μ-oxo) structure ($F = 0$), but they are now located as HOMO−2 and LUMO+1, respectively, so that magnetic exchange is substantially reduced. Consistent with this observation, the lowest-energy triplet state computed for $\mathbf{2}_{100}$ is $^3B_{1u}$, deriving from a b_{2u} to b_{3g} excitation, but the lowest-energy triplet computed for $\mathbf{2}_0$ is $^3B_{3u}$, deriving from a b_{1g} HOMO to b_{2u} LUMO excitation. The relative energies of the magnetically active orbitals in their respective manifolds are quite sensitive to the amount of HF character in the DFT functional, irrespective of structure. Thus, for $\mathbf{2}_{100}$ at the MPW1K level, the b_{2u} HOMO is 0.041 au higher in energy than the b_{1g} HOMO−1 (see Figure 3 for analogous orbital shapes). With the *m*PW1PW91 functional, however, this separation decreases to 0.011 au, and with the pure *m*PWPW91 functional, the energy ordering of these two orbitals is reversed, with the b_{2u} orbital now 0.030 au *below* the now HOMO b_{1g}. This sort of orbital energy positioning proportional to the amount of HF exchange is observed for all structures.

$\{(NH_3)_3Cu\}_2O_2^{2+}$. The energies for structures of **3** as a function of F were computed at all levels of theory using the BS1 basis set, except that (i) the incremental changes on going from the CR-CCSD(T) to CR-CCSD(T)$_L$ level were computed with the BS2 basis set and (ii) consideration of quadruple excitations was not practical at the CC levels. At the CAS and CASPT2 levels, three different active spaces—(8,8), (16,14), and (14,15)—were considered. Results were quite similar for all 3 active spaces, and for the sake of consistency, we only discuss (16,14) results in any detail. At the DFT level, restricted solutions to the Kohn−Sham SCF equations could be obtained for all functionals. With the pure DFT functionals, the RDFT solutions were stable to spin-symmetry breaking with the exception of the TPSS functional, for which BS solutions were found at very slightly lower energy with very small values of $\langle S^2 \rangle$ (less than 0.072) for values of $F \geq 40$. With the hybrid functionals, all structures with $F \geq 40$ were unstable to symmetry breaking. With the *m*PW1PW91 functional, the $F = 20$ solution was also found to be unstable, and at the MPW1K level, the KS solutions for *all* values of F were unstable. Representative relative energies are provided in Table 4, and absolute electronic energies, BS-DFT $\langle S^2 \rangle$ values, and triplet electronic energies for all structures at all levels of theory are in the Supporting Information.

The variation in relative energies as a function of theoretical level returns to being very large for **3**, roughly 90 kcal mol^{-1} for $\mathbf{3}_0$. Once again, the CR-CC and pure DFT levels agree rather well one with another, predicting that $\mathbf{3}_0$ is 4−10 kcal mol^{-1} higher in energy than $\mathbf{3}_{100}$. The agreement is particularly good when the size-extensive and more accurate CR-CCSD(T)$_L$ method is compared with pure DFT. Increased HF character in hybrid functionals is again associated with rapidly increasing relative energies for $\mathbf{3}_0$ and other structures having low values

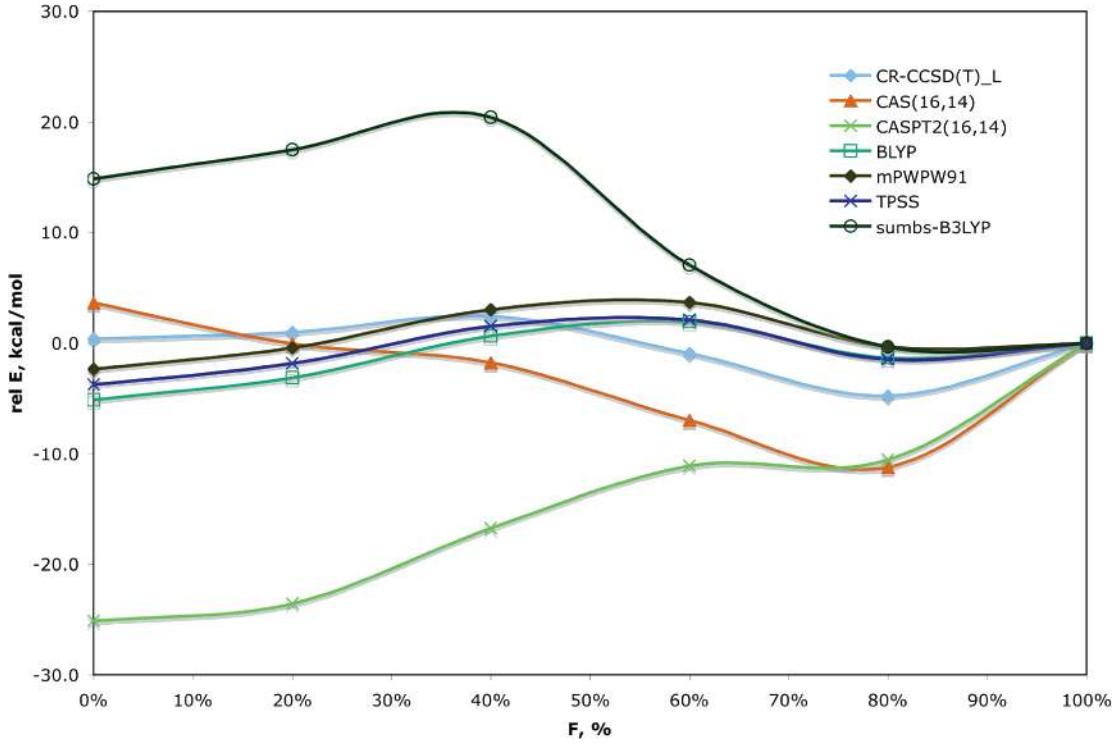

Figure 5. Relative energy (kcal mol^{-1}) vs F for **2** at select levels of theory. (Inset) Legend.

TABLE 4: Relative Energies (kcal mol^{-1}) of 3_F Structures with BS1 Unless Otherwise Noted[a]

	F					
level of theory	0%	20%	40%	60%	80%	100%
CCSD(T)	6.3	6.9	10.3	4.6	−2.4	0.0
CR-CCSD(T)	4.3	5.2	8.2	5.5	−0.4	0.0
CR-CCSD(T)$_L$/BS2	13.1	13.5	14.1	8.2	1.1	0.0
CR-CCSD(T)$_L$[b]	10.1	10.1	11.0	6.2	0.0	0.0
CAS(8,8)	17.9	9.4	3.7	−3.5	−7.7	0.0
CAS(16,14)	29.8	21.0	14.0	3.3	−4.6	0.0
CAS(14,15)	22.5	14.0	9.1	1.1	−5.5	0.0
CASPT2(8,8)	−12.1	−12.2	−7.1	−5.1	−6.4	0.0
	(−17.0)	(−16.1)	(−9.6)	(−6.3)	(−6.8)	(0.0)
CASPT2(16,14)	−17.2	−16.0	−8.4	−5.2	−6.6	0.0
CASPT2(14,15)	−16.6	−15.9	−10.5	−6.0	−6.7	0.0
BLYP	8.4	10.1	13.1	12.4	5.6	0.0
sumBS-B3LYP	26.8	28.8	20.4	14.8	5.0	0.0
*m*PWPW91	9.1	11.1	14.1	13.1	3.1	0.0
TPSS	7.9	9.8	12.2	12.0	3.2	0.0

[a] Values in parentheses correlate all valence electrons and the Cu 3p electrons (44 total), whereas all other non-DFT values refer to the correlation of only the valence electrons (32 total). [b] Computed as CR-CCSD(T)/BS1 + {CR-CCSD(T)$_L$/BS2 − CR-CCSD(T)/BS2}.

of F. The CAS and CASPT2 predictions are again in poor agreement with the CR-CC and pure DFT results and indeed with one another, as the CASPT2 corrections are very large in magnitude and negative for $\mathbf{3}_0$ compared to $\mathbf{3}_{100}$; thus, at the CAS(16,14) level, $\mathbf{3}_0$ is predicted to be 29.8 kcal mol^{-1} *above* $\mathbf{3}_{100}$, whereas at the CASPT2(16,14) level, it is predicted to be 17.2 kcal mol^{-1} *below* $\mathbf{3}_{100}$. These results mimic those of Flock and Pierloot.[30] An interesting technical point is that the CASPT2 energies computed for the (16,14) and (14,15) active spaces with the Cu 3p orbitals treated as formally frozen are in good agreement with the (8,8) active space only when those same orbitals are *not* frozen in the smaller calculation. It appears that the larger active spaces implicitly include some Cu 3p correlation effects.

Figure 6 presents predicted structural relative energies graphically for select levels of theory, including local multireference configuration interaction (MRCI+Q) results from a study of **3** by Rode and Werner (interpolated from energies reported as a function of O−O bond length).[34] It is noteworthy that the sumBS-B3LYP level of theory predicts that the bis(μ-oxo) isomer is higher in energy than the μ-η^2:η^2 peroxo isomer by 26.8 kcal mol^{-1}; this amount is roughly 20 kcal mol^{-1} larger than the predictions made by pure DFT functionals, CR-CC, and MRCI+Q, all of which are in comparatively good agreement with one another. The overall shapes of the pure DFT and CR-CC isomerization curves in Figure 6 are quite similar: the $\mathbf{3}_0$ structure is always predicted to be higher in energy than the $\mathbf{3}_{100}$ structure, and both minima are separated by a relatively low energy barrier in the $F = 40-60$ region. The standard CCSD(T) approach produces a pronounced minimum at $F \approx 80$, which the pure DFT and CR-CCSD(T)$_L$ methods eliminate, making the $\mathbf{3}_{100}$ structure lowest in energy. The CR-CCSD(T) approach produces a very shallow minimum at $F = 80$, but this minimum is located only 0.4 kcal/mol below the $\mathbf{3}_{100}$ structure, making the CR-CCSD(T) potential in the $F = 100$ region quite flat. Geometry optimization at the CR-CCSD(T) level (not possible at this time) might eliminate this shallow minimum at $F = 80$ and shift it to the $F = 100$ region, although it is also possible that the use of the more accurate and rigorously size-extensive CR-CCSD(T)$_L$ level of theory would be required to eliminate this minimum (system **3** is quite big and requires an explicit correlation of at least 80 electrons; the minimum is shallow and can be sensitive to correlation treatment).

The orbitals associated with BS magnetic exchange in **3** are essentially identical to those discussed for **2** (the axial ammonia ligands in **3** make negligible contributions to these orbitals), and the situation with respect to their locations in the occupied and virtual manifolds is also entirely similar. The movement of these orbitals within their respective manifolds as a function of F and percentage of HF exchange in hybrid

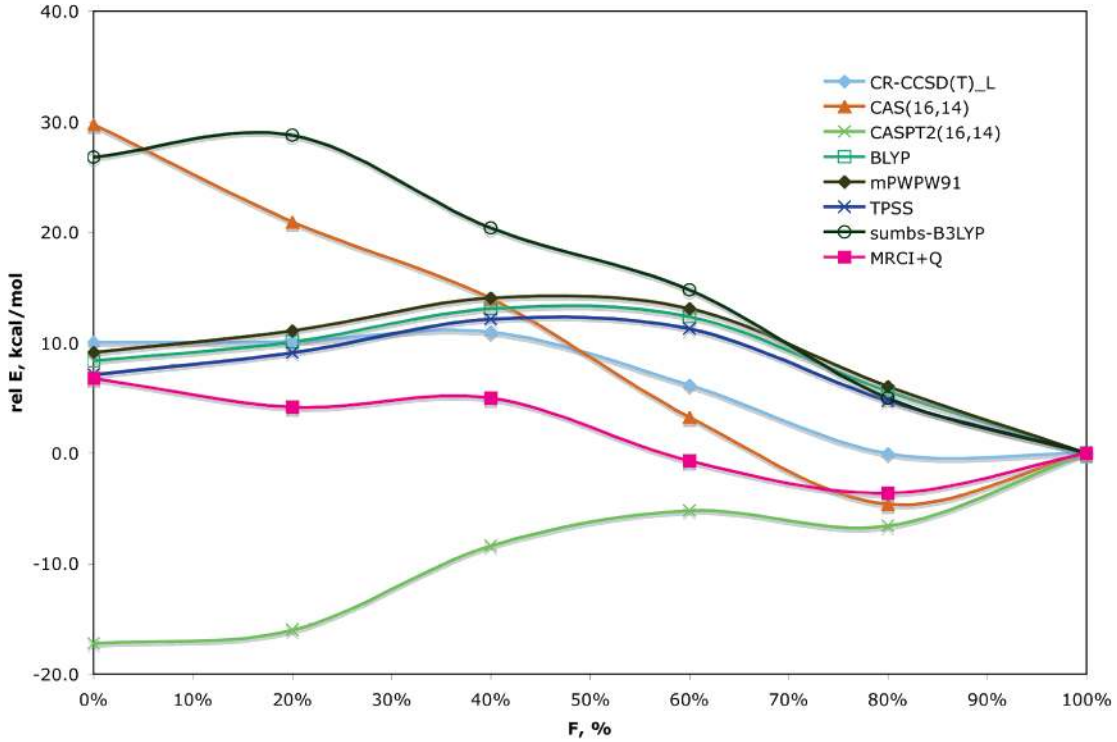

Figure 6. Relative energy (kcal mol^{-1}) vs F for **3** at select levels of theory. (Inset) Legend.

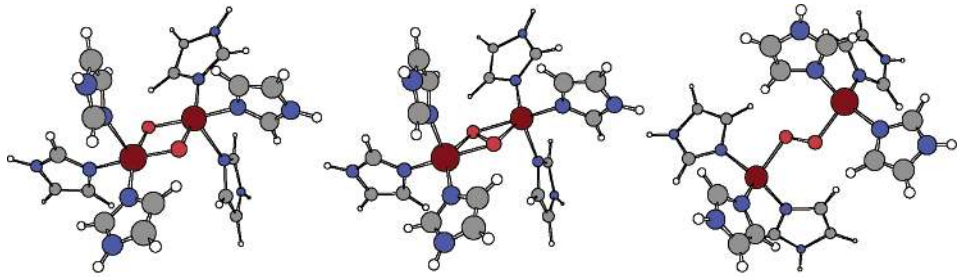

Figure 7. Structures optimized at the BLYP/BS4 level of theory (B3LYP structures are qualitatively identical; all structures belong to the C_i point group).

functionals, together with the lower symmetry for **3** compared to **2**, leads to some technical challenges in obtaining energies for the ^3B_u states that are needed to compute sumBS-DFT energies. In many cases, these triplets are not lowest in energy. Indeed, for small F values, the ^3B_u states corresponding to single occupation of each of these orbitals, formally $|...18a_g^2 17b_u^2 10a_u^2 10b_g^2 11a_u 11b_g\rangle$, prove not even to be the lowest triplet states of B_u symmetry. As noted by Flock and Pierloot,[30] there is a lower-energy ^3B_u configuration, formally $|...18a_g^2 17b_u^2 11a_u^2 9b_g^2 12a_u 10b_g\rangle$. The nonorthogonality of the ^3B_u KS SCF solutions leads to some ambiguity in interpreting sumBS energies, although fortunately the tendency of the hybrid SCF solutions to break symmetry is rather low for small F values where this issue arises (see Supporting Information).

As in **0**−**2**, the CAS orbital occupation numbers for the occupied/virtual pairs analogous to $2b_{3g}/3b_{3g}$ and $4b_{2u}/5b_{2u}$ in Figure 3 change significantly along the isomerization coordinate for **3**. Now the analogous $2b_{3g}/3b_{3g}$ and $4b_{2u}/5b_{2u}$ occupation numbers are 1.78/0.37 and 1.64/0.37 in $\mathbf{3}_0$ and 1.98/0.85 and 1.16/0.07 in $\mathbf{3}_{100}$. The tendency for the μ-η^2:η^2 peroxo isomer to manifest 2 orbitals with occupation numbers very near to 1 is consistent with viewing this species as a nearly pure Cu(II)/Cu(II) singlet biradical.

{(Imid)$_3$Cu}$_2$O$_2^{2+}$. To make more direct contact with the experimentally interesting cases of oxyhemocyanin and oxytyrosinase, we also carried out calculations for **4**. In this case, we did not explore the full isomerization coordinate, owing to the substantial size of the system, nor did we explore many different levels of theory. Instead, we simply optimized bis(μ-oxo) (**4a**), μ-η^2:η^2 peroxo (**4b**), and μ-η^1:η^1 peroxo (**4c**) isomers at the BLYP and B3LYP levels of theory (Figure 7). The former choice was motivated by the excellent performance of the BLYP functional for predicting the isomerization energetics of **0**−**3** in comparison to converged CR-CC results (and, in the case of **3**, in comparison to MRCI+Q). The latter choice was motivated by the substantial use of B3LYP in prior modeling of dicopper−dioxo systems reported in the literature.[30,33,40−43,95]

At both the BLYP and B3LYP levels, **4a** has a stable, restricted KS SCF solution, and analytic frequency calculations verify the structures as true minima. By contrast, at both levels, the KS SCF solution for **4c** is unstable to symmetry breaking (both levels give $\langle S^2\rangle$ values of very nearly 1.0), although the

TABLE 5: Relative Energies (kcal mol^{-1}) of Isomers of 4 with BS4[a]

level of theory	4a	4b	4c
BLYP	8.3	0.0	−0.2 (−1.6)[b]
B3LYP	27.3	0.0 (−0.4)[b]	17.2 (12.3)[b]

[a] The energies for **4c** at the BLYP level and for **4b**,**c** at the B3LYP level are sumBS energies (other cases have stable restricted solutions). Absolute energies may be found in Supporting Information. [b] Relative sumBS energy computed for the structure optimized at the RDFT level of theory.

BS structures are again predicted to be true minima. Finally, the situation is a bit more complicated for **4b**. At the BLYP level, the restricted KS SCF solution is stable and the structure is predicted to have an imaginary frequency of magnitude 4 cm^{-1}. So small an imaginary frequency may quite possibly arise from numerical inaccuracy associated with the quadrature scheme used in evaluating various DFT integrals, or it may legitimately reflect the system's preference to distort to a structure of lower symmetry; but if the latter is the case, the energetic consequence of such a distortion would be expected to be negligible. At the B3LYP level, by contrast, the restricted KS SCF solution is *not* stable. Moreover, even the structure optimized for the BS solution is predicted to have an imaginary frequency of 48 cm^{-1}. The associated normal mode corresponds to movement of the O_2 fragment so as to generate a "butterfly" geometry in the Cu_2O_2 core. Again, however, the rather small magnitude of this frequency suggests that the energetic effects associated with relaxation would be quite small, so we did not reoptimize this structure in C_1 symmetry.

The energies of the various isomers relative to the μ-η^2:η^2 peroxo isomer are provided in Table 5. Consistent with results for **0**−**3**, B3LYP predicts the μ-η^2:η^2 peroxo isomer **4b** to be more stable than the bis(μ-oxo) isomer **4a** by about a 20 kcal mol^{-1} larger margin than does BLYP. The same is true for the energy of **4c** relative to **4a**: the B3LYP prediction is about 17 kcal mol^{-1} larger than that of BLYP.

Discussion

Why do different theoretical methods offer such wildly varying results for the Cu_2O_2 reaction coordinate being studied here? The fundamental challenge is that along the reaction coordinate itself, irrespective of the number or nature of the ligands on the copper, there are large changes in the contributions of dynamical and nondynamical electron correlation to the molecular energies. Nondynamical correlation is associated with the failure of a single determinant to dominate in describing the character of an electronic wave function. A typical example of a system with large nondynamical correlation effects is a singlet biradical, where two determinants (at least) that differ by a double excitation are required for a formally correct description of the singlet configuration. And, indeed, a Cu_2O_2 case in which both copper atoms are Cu(II), as in the μ-η^2:η^2 peroxo isomer, is just such a system if the formally unpaired electrons on each Cu(II) are singlet coupled. Thus, we find CAS calculations predict nearly equal weights (typically about 60:40) for the two dominant singlet configurations of these limiting $F = 100$ isomers of **0**−**3** (this is also consistent with the orbital occupation numbers for $\mathbf{0}_{100}$ and $\mathbf{3}_{100}$ already noted above). Similarly, CC calculations predict that these isomers are each characterized by one very large T_2 cluster amplitude corresponding to a double excitation with both electrons coming from the same occupied orbital and being placed into the same virtual orbital (Table 6; the five largest T_1 and T_2 cluster amplitudes for all geometries may be found in the Supporting Information); in essence, this is an equivalent way of describing what takes place in the CAS calculation. The degree of biradical character drops in every case as the systems transition to the bis(μ-oxo) geometry, as measured by the significant reductions in the weights of the second CAS determinants and the sizes of the corresponding T_2 cluster amplitudes. The diminishment is larger in **2** and **3** than in **0** and **1**, but the trend persists.

TABLE 6: Absolute Values of Dominant T_1 and T_2 Coupled-Cluster Amplitudes for $F = 0$ and $F = 100$ Isomers of 0−3

		T_1		T_2	
molecule	F	amplitude	character	amplitude	character
0	0	0.073	HOMO−1 → LUMO+1	0.187	HOMO−1 → LUMO
	100	0.203	HOMO−4 → LUMO	0.165	HOMO → LUMO
1	0	0.138	HOMO → LUMO+1	0.175	HOMO → LUMO
	100	0.209	HOMO−5 → LUMO	0.209	HOMO → LUMO
2	0	0.197	HOMO → LUMO	0.109	HOMO → LUMO
	100	0.138	HOMO−9 → LUMO	0.228	HOMO → LUMO
3	0	0.215	HOMO → LUMO	0.110	HOMO → LUMO
	100	0.138	HOMO−3 → LUMO	0.270	HOMO → LUMO

However, we find that at the same time as the importance of nondynamical correlation *decreases*, the importance of dynamical correlation significantly *increases*. Dynamical correlation is associated with the degree to which the simultaneous, correlated motion of individual electrons (which reduces their repulsive interaction with one another) is accounted for within the context of a particular theoretical model. Within the CAS formalism, large dynamical correlation effects can be inferred from the presence of many determinants having intermediate weight in the full multireference wave function, even though a single determinant has dominant weight. At the CC level, the equivalent diagnostic is to observe a large number of significant T_1 and T_2 amplitudes, again with no individual amplitude being heavily dominant over all others. Finally, from a purely energetic standpoint, a substantial stabilization of one isomer relative to another upon going from the CAS to the CASPT2 level indicates a greater degree of dynamical correlation in the stabilized species. Again, this is exactly the situation that we observe in all cases, with all dynamical correlation indicators smoothly increasing as F drops to 0. Thus, we may say that the $F = 0$ end of the isomerization path represents a system dominated by dynamical correlation effects, whereas the $F = 100$ end is dominated by nondynamical correlation effects. Flock and Pierloot[30] came to similar conclusions based on their earlier work at the CAS and CASPT2 levels, focusing only on the endpoints of the isomerization coordinate; our CAS and CASPT2 calculations agree well with theirs for these points and establish that the trend is smooth along the full isomerization path, and our CC calculations provide an alternative diagnostic that is entirely consistent with the analysis.

In order, then, to model accurately the Cu_2O_2 isomerization, a method must handle dynamical and nondynamical correlation effects in a well-balanced way. However, there tend to be practical limitations that make achieving such balance decidedly difficult in systems having many electrons. Of the methods employed here, the two that address the correlation problem most rigorously are the CC/CR-CC and CASPT2 levels. In the

abstract, coupled-cluster theory and multireference perturbation theory may be expressed as a series of terms that, in favorable cases, diminish in magnitude and represent at their limits complete solutions to the electronic structure problem. In practice, one must truncate these series expansions in actual systems, but by varying the point of truncation, one can gain insight into the convergence of the expansion used. With respect to CC and CR-CC methods, one degree of convergence is associated with the inclusion of higher-order cluster components (triples, quadruples, etc.) in the calculations. We observe the effect of quadruple excitations to be quite small once the complete renormalization of the energy corrections to CCSD energies due to higher-than-double excitations is accomplished, suggesting that this aspect of the calculation is well converged. The standard single-reference CC methods, such as CCSD(T) and CCSD(TQ), do not show the same level of convergence, but this is because they fail to describe biradical and other quasi-degenerate systems. The failure of standard CC methods is a consequence of the poor convergence of MBPT, which is used to define the (T) and (TQ) corrections in the CCSD(T) and CCSD(TQ) schemes. The CR-CCSD(T), CR-CCSD(TQ), and CR-CCSD(T)$_L$ methods renormalize the noniterative energy corrections due to triples and quadruples in a manner consistent with the degree of biradical character of the system under consideration and eliminate, in this way, the failures of the standard CC methods in cases involving biradicals and larger nondynamical correlation effects.[72−87] The use of the most recent, rigorously size-extensive CR-CCSD(T)$_L$ formalism, which should increase the quality of the computed CR-CCSD(T) energies even further, makes relatively small changes in the CR-CC isomerization curves, suggesting that size extensivity errors in the CR-CCSD(T) calculations are small and that the higher-order effects included in the CR-CCSD(T)$_L$ calculations are in most cases relatively small as well, confirming our earlier statements that the CR-CC calculations are converged.

With respect to CAS and CASPT2, the situation is less clear. When CAS active spaces are expanded to their practical limit of (16,14), there appears to be, in general, a reasonably good convergence in the isomerization potential-energy curves. Thus, for example, comparing (8,8), (16,14), and (14,15) results, the CASPT2 relative energies are consistent to within 1 or 2 kcal mol^{-1}. However, accounting for dynamical correlation effects at the CASPT2 level tends to lead to very large changes in the predicted energetics of isomerization relative to the CASSCF level, particularly for **3** where an inversion in relative energies of 48 kcal mol^{-1} is observed comparing $F = 0$ to $F = 100$. Siegbahn,[95] commenting on the prior work of Flock and Pierloot[30] for **3**, has suggested that such an observation should be treated as an indication that CASPT2 is not appropriate for the subject system. Rode and Werner,[34] employing a local multireference CI approach to compute dynamical correlation energy, predicted a much smaller stabilization energy for $F = 0$ compared to $F = 100$ than that predicted at the CASPT2 level (Figure 6), coming up with a final relative energy that is in fairly good agreement with our best CR-CCSD(T)$_L$ estimates (6−8 kcal mol^{-1} after considering various additive corrections from other computations). The (6,8) active space employed to generate the CAS reference for the MRCI was rather small on the basis of our experience with **3** (where an inspection of the orbital occupation numbers for much larger active spaces indicates none of the orbitals to be unimportant); thus, the very close agreement between the two levels may be in part fortuitous, but it is there nevertheless.

Although we have explored the active space in some detail, and indeed have reached a practical limit in terms of size, it is possible that improved results might be obtained by swapping certain virtual orbitals with others constructed primarily from Cu 4d functions, thereby correlating Cu d electrons to a greater extent at the expense of those occupied orbitals dominated by the basis functions of the first-row atoms. However, the active space used previously by Flock and Pierloot[30] did include one Cu 4d virtual orbital and their results were very similar to ours. It is also conceivable that an explicit accounting for relativistic effects with an all-electron basis set might lead to improved results. Finally, optimization of the molecular geometries at the CASPT2 level could lead to improved relative energetics; the lack of analytic CASPT2 gradients makes it difficult to evaluate this point. In any case, like Flock and Pierloot[30] and Rode and Werner,[34] we find that informed use of the single-root CASPT2 model fails to provide results consistent with other levels of theory.

However, given the highly biradical nature of many of the structures, particularly those with large values of F, it may be that improved energies could be obtained by including more electronic states in a CASSCF state-average calculation and then permitting them to interact via the multistate (MS) CASPT2 formalism (this method takes into account the coupling of several electronic states at second order via an effective Hamiltonian, the diagonalization of which provides improved state energies[96]). Time-dependent (TD) DFT calculations at the BLYP level indicate that for **3**, for instance, there is a totally symmetric excited singlet state within 1.05 eV of the ground state for the $F = 100$ structure. For the $F = 0$ structure, on the other hand, the first totally symmetric excited singlet state is 1.54 eV higher in energy than the ground state. State interaction would therefore be expected to lower the energy of the peroxo form relative to the bis-μ-oxo, which is in the direction needed to improve agreement with the CR-CC, pure DFT, and MRCI levels of theory—unpublished work by another group suggests that this occurs.[97] However, the situation is less clear with **0**−**2**. In the case of **2**, TD DFT predicts that neither isomer has an excited singlet state belonging to the totally symmetric irrep within 3 eV of the ground state. Each isomer *does* have a first excited singlet state 1.2 eV above the ground state ($^1B_{3u}$ for $F = 0$ and $^1B_{2g}$ for $F = 100$), but any multistate interaction would have to derive from vibrational coupling, and such matrix elements are not trivially calculated. For **0** and **1**, the instability of their restricted KS SCF solutions mitigates against application of the TD formalism. Given the significant technical issues and the activities of other authors,[97] we defer any further consideration of MS CASPT2 calculations.

Interestingly, results predicted from DFT calculations using pure functionals (BLYP, *m*PWPW91, and TPSS) are in very good agreement with CR-CC (and with MRCI, for the case of **3**) but they are not with CASPT2. Analysis of the DFT results is less straightforward than with the other levels of theory because different DFT functionals *cannot* be analyzed in terms of a series of hopefully convergent terms. However, the trends observed for the functionals, as a function of the percentage of HF exchange that they include, provide some insight into their performance.

One key observation is the failure of the pure functionals to break restricted spin symmetry in **2** and **3**, even for the $F = 100$ isomer. By contrast, with increasing HF character, the hybrid functionals all give lower-energy unrestricted solutions for $F = 100$, and indeed the point along the isomerization curve from $F = 0$ to $F = 100$ at which they break sym-

metry is inversely proportional to the percentage of HF exchange that they contain. The instability of a restricted solution relative to an unrestricted solution is often associated with the inadequacy of a single KS determinant to describe a singlet biradical. This analysis is entirely consistent with the results noted above, where the energy separation between the magnetically correlating orbitals of Figure 3 was observed to be inversely proportional to the amount of HF exchange in a hybrid functional.

Cremer and co-workers have extensively analyzed the performance of various functionals in the context of biradicals and concluded that pure functionals, by *not* incorporating any HF exchange, take a greater account of nondynamical correlation intrinsically within their formulation than do hybrid functionals.[98−101] They are thus more stable to symmetry breaking and, at least on the basis of comparison to CR-CC, seem to be very well balanced in *all* of the systems studied here with respect to their ability to account for *variations* in both dynamical and nondynamical correlation (even in **0** and **1**, where *all* functionals prove unstable to symmetry breaking).

Inclusion of HF exchange, then, with its associated increased tendency to spin-symmetry breaking, seems to overstabilize the μ-η^2:η^2 peroxo isomer relative to the bis(μ-oxo), with the magnitude of that destabilization being anywhere from 5 to 10 kcal mol^{-1} for every 10% of HF exchange included in the functional—a surprisingly large and chemically important error that mitigates against the use of hybrid functionals in these systems. Rode and Werner[34] noted this same effect comparing BLYP to B3LYP for **3**, and the present results indicate that it is largely independent of the choice of exchange and correlation functionals.

Although an internal comparison of theoretical levels can be instructive, we would be remiss were we not also to consider the data within the context of experimental knowledge. Molecules **0**−**3** are fictional in the sense that ammonia is not a ligand that has yet found use in experimental systems. However, many analogues of **2** and **3** have been characterized at this point,[12,15] and their structural preferences are reasonably well established. For instance, analogues of **2** inevitably prefer bis(μ-oxo) geometries relative to μ-η^2:η^2 peroxo alternatives. This is consistent with our pure DFT and CR-CC results, which predict **2** to be the only system in which bis(μ-oxo) $F = 0$ is indeed preferred over $F = 100$. With respect to **3**, examples of both coordination geometries are known, and the μ-η^2:η^2 peroxo form seems to be preferred when tridentate ligands are employed that are not sterically constrained to coordinate to Cu in a roughly square-pyramidal fashion (inspection of Figure 7, for instance, illustrates how the imidazole N atoms are displaced out of the core plane in the μ-η^2:η^2 peroxo form but essentially perfectly in the plane for the bis(μ-oxo) form). On the basis of previous DFT studies of analogues of **3** coordinated to triazacyclononane ligands, Bercès emphasized the importance of ligand constraints in the stabilization of bis(μ-oxo) geometries.[28] Thus, the predictions of pure DFT, CR-CC, and MRCI that unconstrained **3** prefers the μ-η^2:η^2 peroxo, but only by a small margin that could readily be overcome by ligand effects, again seems consistent with experiment. (We note that prior continuum solvation calculations for a medium characterized by a dielectric constant of 10 have predicted the bis(μ-oxo) form of **3** to be better solvated than the μ-η^2:η^2 peroxo by 6−8 kcal mol^{-1};[27] this differential solvation would be expected to be diminished with larger ligands, which more effectively descreen the solute from the solvent, but any remaining preference for the bis(μ-oxo) form would reduce the degree to which ligand strain would be needed to shift the equilibrium between the two forms.)

Some final points of comparison between DFT and the wave-function models are noteworthy. Correlation of the 12 Cu 3p electrons makes the wave-function methods more expensive, and in those cases where we could practically do so the effect was variable: relative to $F = 100$, the $F = 0$ isomer increased by about 5 kcal mol^{-1} at the CR-CC and CASPT2 levels for **0**, decreased by 1 kcal mol^{-1} at the CASPT2 level for **1**, and decreased by 4 kcal mol^{-1} at the CASPT2 level for **2**. By contrast, the DFT level includes the correlation of these electrons (and indeed *all* electrons) by construction. In addition, most of the wave-function methods predict $F = 80$ structures to be lower in relative energy, sometimes by a large margin, than corresponding predictions at the DFT level. If we consider **3**, which is the most informative system to examine because the geometries of $\mathbf{3}_0$ and $\mathbf{3}_{100}$ were fully optimized at the B3LYP level, most DFT models predict a relative energy for $\mathbf{3}_{80}$ of about 5 kcal mol^{-1}. The correlated level in best agreement with this prediction is the CR-CCSD(T)$_L$/BS2 level, which predicts a relative energy of 1.1 kcal mol^{-1} for $\mathbf{3}_{80}$; the other CR-CC models predict values closer to 0.0. However, the remaining correlated levels predict the $F = 80$ structure to be lower in energy than the $F = 100$ structure, which is a highly suspect result because $F = 80$ structures have O−O bond lengths on the order of 1.6 Å, and this is considerably longer than is observed in any experimentally known μ-η^2:η^2 peroxo isomer.[12,15]

In summary, then, the experimental and theoretical data appear to support the use of *pure* DFT functionals for the modeling of Cu_2O_2 systems, especially if larger ligands are to be modeled that render the otherwise quantitatively similar CR-CC or MRCI methods less practical at this time. Hybrid DFT, standard CC, and single-root CASPT2 calculations are not useful in this context. Given the utility of the reasonably well converged CR-CC results as benchmarks for systems **0**−**3**, and in particular of the newly developed size-extensive CR-CCSD(T)$_L$ method, there is a strong motivation to develop local variants of these approaches so that they may be applied to metalloenzyme models with more realistic ligands.

We may turn at last, then, to the issue of imidazole as a ligand and the implications for the mechanism of oxytyrosinase. Flock and Pierloot[30] originally suggested, on the basis of their CASPT2 prediction of a preferred bis(μ-oxo) form for **3**, that the experimental observation of a μ-η^2:η^2 peroxo isomer in the active site of oxyhemocyanin must arise from steric effects associated with the larger imidazole ligands. However, the energy differences between the two isomers of **3** and **4** are predicted to be almost identical at the BLYP level: 8.4 vs 8.3 kcal mol^{-1}. As Figure 7 illustrates, torsions of the imidazole rings make steric interactions negligible, and instead we must continue to conclude that the pure DFT functional is likely to be correct in predicting that the fictional system **3** prefers the μ-η^2:η^2 peroxo form, whereas single-root CASPT2 is in error. Importantly, however, the *hybrid* B3LYP functional continues to underestimate the stability of the bis(μ-oxo) isomer relative to the μ-η^2:η^2 peroxo isomer by about 20 kcal mol^{-1}. Thus, prior studies of oxytyrosinase at the B3LYP level[42,43,95] that discounted C−H bond-activation pathways passing through a bis(μ-oxo) intermediate because of its (erroneously) high energy may merit reinvestigation with a more robust pure functional. Recent results of Mirica et al.,[40] on the other hand, where a B3LYP transition-state structure for C−H bond activation from a bis(μ-oxo) geometry was found to be lower in energy than a

transition-state structure for isomerization to a μ-η^2:η^2 peroxo form for a particular ligand system, may be considered to remain qualitatively correct, although the magnitude of the preference for the C−H abstraction pathway may be larger than is predicted at the B3LYP level.

Acknowledgment. This work was supported by the National Science Foundation (CHE-9974834, CHE-0203346, and CHE-0309517), the Chemical Sciences, Geosciences, and Biosciences Division, Office of Basic Energy Sciences, Office of Science, U.S. Department of Energy (Grant No. DE-FG02-01ER15228), and the High Performance Computing Center at Michigan State University. Professors Björn Roos, Peter Taylor, and Bill Tolman are thanked for stimulating discussions. We thank Hans-Joachim Werner for providing us with a preprint of ref 34. P.P. and M.W. appreciate the assistance of Mr. Andrew Keen and Dr. Armagan Kinal in the CC calculations performed in this work. Finally, P.P. acknowledges the support offered by the Invited Fellowship of the Japan Society for the Promotion of Science during his two-month tenure as Visiting Professor at Kyoto University and useful discussions with his host, Professor Hiroshi Nakatsuji.

Supporting Information Available: Cartesian coordinates, absolute (singlet and triplet) and relative electronic energies at all levels of theory for all structures, BS-DFT $\langle S^2 \rangle$ values, and additional technical details on theoretical models. This material is available free of charge via the Internet at http://pus.acs.org.

References and Notes

(1) Solomon, E. I.; Baldwin, M. J.; Lowery, M. D. *Chem. Rev.* **1992**, *92*, 521.
(2) Kitajima, N.; Moro-oka, Y. *Chem. Rev.* **1994**, *94*, 737.
(3) Fox, S.; Karlin, K. D. In *Active Oxygen in Biochemistry*; Valentine, J. S., Foote, C. S., Greenberg, A., Liebman, J. F., Eds.; Blackie Academic & Professional, Chapman & Hall: Glasgow, Scotland, 1995; p 188.
(4) Kaim, W.; Rall, J. *Angew. Chem., Int. Ed. Engl.* **1996**, *35*, 43.
(5) Klinman, J. P. *Chem. Rev.* **1996**, *96*, 2541.
(6) Solomon, E. I.; Sundaram, U. M.; Machonkin, T. E. *Chem. Rev.* **1996**, *96*, 2563.
(7) Solomon, E. I.; Chen, P.; Metz, M.; Lee, S.-K.; Palmer, A. E. *Angew. Chem., Int. Ed.* **2001**, *40*, 4570.
(8) Gamez, P.; Koval, I. A.; Reedijk, J. *Dalton Trans.* **2004**, 4079.
(9) Decker, H.; Dillinger, R.; Tuczek, F. *Angew. Chem., Int. Ed.* **2000**, *39*, 1591.
(10) Solomon, E. I.; Tuczek, F.; Root, D. E.; Brown, C. A. *Chem. Rev.* **1994**, *94*, 827.
(11) Tolman, W. B. *Acc. Chem. Res.* **1997**, *30*, 227.
(12) Mirica, L. M.; Ottenwaelder, X.; Stack, T. D. P. *Chem. Rev.* **2004**, *104*, 1013.
(13) Lewis, E. A.; Tolman, W. B. *Chem. Rev.* **2004**, *104*, 1047.
(14) Cole, A. P.; Mahadevan, V.; Mirica, L. M.; Ottenwaelder, X.; Stack, T. D. P. *Inorg. Chem.* **2005**, *44*, 7345.
(15) Stack, T. D. P. *Dalton Trans.* **2003**, 1881.
(16) Jung, B.; Karlin, K. D.; Zuberbühler, A. D. *J. Am. Chem. Soc.* **1996**, *118*, 3763.
(17) Holland, P. L.; Tolman, W. B. *Coord. Chem. Rev.* **1999**, *192*, 855.
(18) Magnus, K. A.; Ton-That, H.; Carpenter, J. E. *Chem. Rev.* **1994**, *94*, 727.
(19) Magnus, K. A.; Hazes, B.; Ton-That, H.; Bonaventura, C.; Bonaventura, J.; Hol, W. G. J. *Proteins: Struct., Funct., Genet.* **1994**, *19*, 302.
(20) Cahoy, J.; Holland, P. L.; Tolman, W. B. *Inorg. Chem.* **1999**, *38*, 2161.
(21) Que, L.; Tolman, W. B. *Angew. Chem., Int. Ed.* **2002**, *41*, 1114.
(22) Pidcock, E.; DeBeer, S.; Obias, H. V.; Hedman, B.; Hodgson, K. O.; Karlin, K. D.; Solomon, E. I. *J. Am. Chem. Soc.* **1999**, *121*, 1870.
(23) Liang, H.-C.; Zhang, C. X.; Henson, M. J.; Sommer, R. D.; Hatwell, K. R.; Kaderli, S.; Zuberbühle, A. D.; Rheingold, A. L.; Solomon, E. I.; Karlin, K. D. *J. Am. Chem. Soc.* **2002**, *124*, 4170.
(24) Henson, M. J.; Vance, M. A.; Zhang, C. X.; Liang, H. C.; Karlin, K. D.; Solomon, E. I. *J. Am. Chem. Soc.* **2003**, *125*, 5186.
(25) Mizuno, M.; Hayashi, H.; Fujinami, S.; Furutachi, H.; Nagatomo, S.; Otake, S.; Uozumi, K.; Suzuki, M.; Kitagawa, T. *Inorg. Chem.* **2003**, *42*, 8534.
(26) Liang, H. C.; Henson, M. J.; Hatcher, L. Q.; Vance, M. A.; Zhang, C. X.; Lahti, D.; Kaderli, S.; Sommer, R. D.; Rheingold, A. L.; Zuberbuhler, A. D.; Solomon, E. I.; Karlin, K. D. *Inorg. Chem.* **2004**, *43*, 4115.
(27) Cramer, C. J.; Smith, B. A.; Tolman, W. B. *J. Am. Chem. Soc.* **1996**, *118*, 11283.
(28) Bérces, A. *Inorg. Chem.* **1997**, *36*, 4831.
(29) Yoshizawa, K.; Ohta, T.; Yamabe, T. *Bull. Chem. Soc. Jpn.* **1997**, *70*, 1911.
(30) Flock, M.; Pierloot, K. *J. Phys. Chem. A* **1999**, *103*, 95.
(31) Lam, B. M. T.; Halfen, J. A.; Young, V. G., Jr.; Hagadorn, J. R.; Holland, P. L.; Lledos, A.; Cucurull-Sanchez, L.; Novoa, J. J.; Alvarez, S.; Tolman, W. B. *Inorg. Chem.* **2000**, *39*, 4059.
(32) Henson, M. J.; Mukherjee, P.; Root, D. E.; Stack, T. D. P.; Solomon, E. I. *J. Am. Chem. Soc.* **1999**, *121*, 10332.
(33) Siegbahn, P. E. M. *J. Biol. Inorg. Chem.* **2003**, *8*, 577.
(34) Rode, M. F.; Werner, H.-J. *Theor. Chem. Acc.* **2005**, *114*, 309.
(35) Steinfeld, J. I.; Francisco, J. S.; Hase, W. L. *Chemical Kinetics and Dynamics*, 2nd ed.; Prentice Hall: New York, 1999.
(36) Hatcher, L. Q.; Karlin, K. D. *J. Biol. Inorg. Chem.* **2004**, *9*, 669.
(37) Cramer, C. J.; Pak, Y. *Theor. Chem. Acc.* **2001**, *105*, 477.
(38) Cramer, C. J.; Kinsinger, C. K.; Pak, Y. *J. Mol. Struct. (THEOCHEM)* **2003**, *632*, 111.
(39) Spuhler, P.; Holthausen, M. C. *Angew. Chem., Int. Ed.* **2003**, *42*, 5961.
(40) Mirica, L. M.; Vance, M.; Rudd, D. J.; Hedman, B.; Hodgson, K. O.; Solomon, E. I.; Stack, T. D. P. *Science* **2005**, *308*, 1890.
(41) Lind, T.; Siegbahn, P. E. M.; Crabtree, R. H. *J. Phys. Chem. B* **1999**, *103*, 1193.
(42) Siegbahn, P. E. M.; Wirstam, M. *J. Am. Chem. Soc.* **2001**, *123*, 11819.
(43) Siegbahn, P. E. M. *J. Biol. Inorg. Chem.* **2003**, *8*, 567.
(44) Dolg, M.; Wedig, U.; Stoll, H.; Preuss, H. *J. Chem. Phys.* **1987**, *86*, 866.
(45) Pierloot, K.; Dumez, B.; Widmark, P.-O.; Roos, B. O. *Theor. Chim. Acta* **1995**, *90*, 87.
(46) Hehre, W. J.; Radom, L.; Schleyer, P. v. R.; Pople, J. A. *Ab Initio Molecular Orbital Theory*; Wiley: New York, 1986.
(47) Easton, R. E.; Giesen, D. J.; Welch, A.; Cramer, C. J.; Truhlar, D. G. *Theor. Chim. Acta* **1996**, *93*, 281.
(48) Becke, A. D. *Phys. Rev. A* **1988**, *38*, 3098.
(49) Lee, C.; Yang, W.; Parr, R. G. *Phys. Rev. B* **1988**, *37*, 785.
(50) Perdew, J. P. In *Electronic Structure of Solids '91*; Ziesche, P., Eschrig, H., Eds.; Akademie Verlag: Berlin, 1991; p 11.
(51) Perdew, J.; Wang, Y. *Phys. Rev. B* **1992**, *45*, 13244.
(52) Adamo, C.; Barone, V. *J. Chem. Phys.* **1998**, *108*, 664.
(53) Tao, J.; Perdew, J. P.; Staroverov, V. N.; Scuseria, G. E. *Phys. Rev. Lett.* **2003**, *91*, 146401.
(54) Becke, A. D. *J. Chem. Phys.* **1993**, *98*, 5648.
(55) Stephens, P. J.; Devlin, F. J.; Chabalowski, C. F.; Frisch, M. J. *J. Phys. Chem.* **1994**, *98*, 11623.
(56) Lynch, B. J.; Fast, P. L.; Harris, M.; Truhlar, D. G. *J. Phys. Chem. A* **2000**, *104*, 4811.
(57) Staroverov, V. N.; Scuseria, G. E.; Tao, J.; Perdew, J. P. *J. Chem. Phys.* **2003**, *119*, 12129.
(58) Cramer, C. J. *Essentials of Computational Chemistry*, 2nd ed.; John Wiley & Sons: Chichester, UK, 2004.
(59) Ziegler, T.; Rauk, A.; Baerends, E. J. *Theor. Chim. Acta* **1977**, *43*, 261.
(60) Yamaguchi, K.; Jensen, F.; Dorigo, A.; Houk, K. N. *Chem. Phys. Lett.* **1988**, *149*, 537.
(61) Lim, M. H.; Worthington, S. E.; Dulles, F. J.; Cramer, C. J. In *Chemical Applications of Density Functional Theory*; Laird, B. B., Ross, R. B., Ziegler, T., Eds.; American Chemical Society: Washington, DC, 1996; Vol. 629, p 402.
(62) Isobe, H.; Takano, Y.; Kitagawa, Y.; Kawakami, T.; Yamanaka, S.; Yamaguchi, K.; Houk, K. N. *Mol. Phys.* **2002**, *100*, 717.
(63) Gräfenstein, J.; Cremer, D. *Mol. Phys.* **2001**, *99*, 981.
(64) Čížek, J. *J. Chem. Phys.* **1966**, *45*, 4256.
(65) Čížek, J. *Adv. Chem. Phys.* **1969**, *14*, 35.
(66) Purvis, G. D.; Bartlett, R. J. *J. Chem. Phys.* **1982**, *76*, 1910.
(67) Scuseria, G. E.; Scheiner, A. C.; Lee, T. J.; Rice, J. E.; Schaefer, H. F., III. *J. Chem. Phys.* **1987**, *86*, 2881.
(68) Piecuch, P.; Paldus, J. *Int. J. Quantum Chem.* **1989**, *36*, 429.
(69) Raghavachari, K.; Trucks, G. W.; Pople, J. A.; Head-Gordon, M. *Chem. Phys. Lett.* **1989**, *157*, 479.
(70) Kowalski, K.; Piecuch, P. *J. Chem. Phys.* **2000**, *113*, 5644.
(71) Özkan, I.; Kinal, A.; Balci, M. *J. Phys. Chem. A* **2004**, *108*, 507.
(72) McGuire, M. J.; Piecuch, P. *J. Am. Chem. Soc.* **2005**, *127*, 2608.
(73) Kinal, A.; Piecuch, P. *J. Phys. Chem. A* **2006**, in press.

(74) Piecuch, P.; Kowalski, K. In *Computational Chemistry: Reviews of Current Trends*; Leszczyn ski, J., Ed.; World Scientific: Singapore, 2000; Vol. 5, p 1.
(75) Kowalski, K.; Piecuch, P. *J. Chem. Phys.* **2000**, *113*, 18.
(76) Kowalski, K.; Piecuch, P. *Chem. Phys. Lett.* **2001**, *344*, 165.
(77) Piecuch, P.; Kucharski, S. A.; Špirko, V.; Kowalski, K. *J. Chem. Phys.* **2001**, *115*, 5796.
(78) McGuire, M. J.; Kowalski, K.; Piecuch, P. *J. Chem. Phys.* **2002**, *117*, 3617.
(79) McGuire, M. J.; Piecuch, P.; Kowalski, K.; Kucharski, S. A.; Musiał, M. *J. Phys. Chem. A* **2004**, *108*, 8878.
(80) Kowalski, K.; Piecuch, P. *J. Chem. Phys.* **2005**, *122*, 074107.
(81) Piecuch, P.; Kowalski, K.; Pimienta, I. S. O.; Kucharski, S. A. In *Low-Lying Potential Energy Surfaces*; Hoffmann, M. R., Dyall, K. G., Eds.; American Chemical Society: Washington, DC, 2002; Vol. 828, p 31.
(82) Piecuch, P.; Kowalski, K.; Pimienta, I. S. O.; McGuire, M. J. *Int. Rev. Phys. Chem.* **2002**, *21*, 527.
(83) Piecuch, P.; Pimienta, I. S. O.; Fan, P.-D.; Kowalski, K. In *Progress in Theoretical Chemistry and Physics*; Maruani, J., Lefebvre, R., Brändas, E., Eds.; Kluwer: Dordrecht, Netherlands, 2003; Vol. 12, p 119.
(84) Piecuch, P.; Kowalski, K.; Pimienta, I. S. O.; Fan, P.-D.; Lodriguito, M.; McGuire, M. J.; Kucharski, S. A.; Kuś, T.; Musiał, M. *Theor. Chem. Acc.* **2004**, *112*, 349.
(85) Piecuch, P.; Włoch, M.; Lodriguito, M.; Gour, J. R. In *Progress in Theoretical Chemistry and Physics*; Wilson, S., Julien, J.-P., Maruani, J., Brändas, E., Delgado-Barrio, G., Eds.; Springer: Berlin, 2006, in press; Vol. 15.
(86) Piecuch, P.; Włoch, M. *J. Chem. Phys.* **2005**, *123*, 224105.
(87) Piecuch, P.; Włoch, M.; Gour, J. R.; Kinal, A. *Chem. Phys. Lett.* **2005**, *418*, 463.
(88) Roos, B. O. In *Ab Initio Methods in Quantum Chemistry*; Lawley, K. P., Ed.; Wiley: New York, 1987; Vol. 2, p 399.
(89) Andersson, K.; Malmqvist, P.-Å.; Roos, B. O.; Sadlej, A. J.; Wolinski, K. *J. Phys. Chem.* **1990**, *94*, 5483.
(90) Persson, B. J.; Roos, B. O.; Pierloot, K. *J. Chem. Phys.* **1994**, *101*, 6810.
(91) Gagliardi, L.; Roos, B. O. *Inorg. Chem.* **2003**, *42*, 1599.
(92) Ghosh, A.; Taylor, P. R. *Curr. Opin. Chem. Biol.* **2003**, *7*, 113.
(93) Roos, B. O.; Andersson, K.; Fülscher, M. P.; Serrano-Andrés, L.; Pierloot, K.; Merchán, M.; Molina, V. *J. Mol. Struct. (THEOCHEM)* **1996**, *388*, 257.
(94) Ghigo, G.; Roos, B. O.; Malmqvist, P.-Å. *Chem. Phys. Lett.* **2004**, *396*, 142.
(95) Siegbahn, P. E. M. *Quart. Rev. Biophys.* **2003**, *36*, 91.
(96) Finley, J.; Malmqvist, P.-Å.; Roos, B. O.; Serrano-Andres, L. *Chem. Phys. Lett.* **1998**, *288*, 299.
(97) Roos, B. O., personal communication.
(98) He, Y.; Gräfenstein, J.; Kraka, E.; Cremer, D. *Mol. Phys.* **2000**, *98*, 1639.
(99) Polo, V.; Kraka, E.; Cremer, D. *Theor. Chem. Acc.* **2002**, *107*, 291.
(100) Gräfenstein, J.; Kraka, E.; Filatov, M.; Cremer, D. *Int. J. Mol. Sci.* **2002**, *3*, 360.
(101) Gräfenstein, J.; Cremer, D. *Mol. Phys.* **2005**, *103*, 279.